# Supporting Information – “Hole-Transport in Low-Donor-Content Organic Solar Cells”

Donato Spoltore[1,*], Andreas Hofacker[1], Johannes Benduhn[1], Sascha Ullbrich[1], Mathias Nyman[2], Olaf Zeika[1], Sebastian Schellhammer[3,4], Yeli Fan[5,+], Ivan Ramirez[6,x], Stephen Barlow[5], Moritz Riede[6], Seth R. Marder[5], Frank Ortmann[3], Koen Vandewal[1,§,*]

1. Dresden Integrated Center for Applied Physics and Photonic Materials (IAPP) and Institute for Applied Physics, Technische Universität Dresden, 01187 Dresden, Germany
2. Physics, Faculty of Science and Engineering, Åbo Akademi University, Porthansgatan 3, 20500 Turku, Finland
3. Center for Advancing Electronics (cfaed), Technische Universität Dresden, 01062 Dresden, Germany
4. Institute for Materials Science and Max Bergmann Center of Biomaterials, Technische Universität Dresden, 01062 Dresden, Germany
5. Center for Organic Photonics and Electronics and School of Chemistry and Biochemistry, Georgia Institute of Technology, Atlanta, Georgia 30332-0400, United States
6. Department of Physics, Oxford of University, Parks Road OX1 3PU Oxford, United Kingdom

+ Current address: School of Chemistry and Chemical Engineering, Southeast University, Nanjing 211189, Jiangsu, P.R. China

x Current address: Heliatek GmbH, Treidlerstraße 3, 01139 Dresden, Germany

§ Current address: Institute for Materials Research (IMO-IMOMEC), Hasselt University, Wetenschapspark 1, 3590 Diepenbeek, Belgium

* Corresponding authors: donato.spoltore@iapp.de, koen.vandewal@uhasselt.be

# 1. List of Donor Materials

Table S1. Information on the donor materials used in low-donor-content organic solar cells. $C_{60}$ is used as acceptor (94 mol%). The energy of the charge transfer (CT) state ($E_{CT}$) and the reorganization energy ($\Lambda_{DA}^{exp}$) were obtained by fitting the low energy region of the CT absorption band measured by sensitive EQE. The indicated error values are obtained by a systematic variation of the fitting range.

| Nr. | Donor (Supplier) | Structure and Chemical Name | Hole μ [$cm^2\ V^{-1}\ s^{-1}$] | exp. $E_{CT}$ [meV] | $\Lambda_{DA}^{exp}$ [meV] | $\Lambda_{D}^{calc}$ [meV] | $\Lambda_{D}^{\prime calc}$ [meV] | DFT IPs [eV] |
|---|---|---|---|---|---|---|---|---|
| **1** | **Rubrene** (Sensient) | 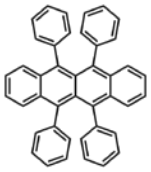 5,6,11,12-tetraphenyl-tetracene | 6.61E-5 | 1464 ±1 | 80 ±3 | 89 | 38 | 5.38 |
| **2** | **P4-Ph4-DIP** (TU Dresden) | 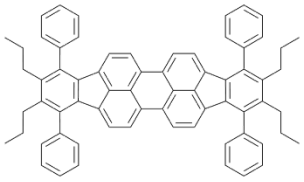 2,3,10,11-tetrapropyl-1,4,9,12-tetraphenyl-diindeno[1,2,3-*cd*:1',2',3'-*lm*]perylene | 5.68E-6 | 1608 ±1 | 102 ±4 | 62 | 14 | 5.66 |
| **3** | **BP-Bodipy** (TU Dresden) | 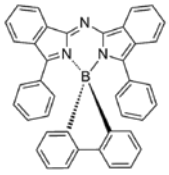 10',14'-diphenyl-5λ⁴,11'λ⁴-spiro[dibenzo[*b,d*]borole-5,12'-[1,3,5,2]1,3,5,2]triazaborinino[4,3-*a*:6,1-a'] diisoindole] | 4.50E-5 | 1453 ±1 | 125 ±4 | 83 | 43 | 5.40 |
| **4** | **TPDP** (TU Dresden) | 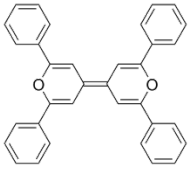 2,2',6,6'-tetraphenyl-4,4'-bipyranylidene | 2.42E-5 | 913 ±1 | 164 ±5 | 143 | 38 | 4.69 |

| | | | | | | | | |
|---|---|---|---|---|---|---|---|---|
| **5** | **TAPC** (Sensient) | 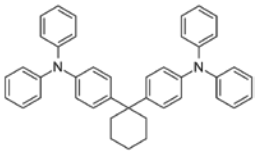 1,1-bis[4-(*N*,*N*-di-*p*-tolylamino)phenyl]cyclohexane | 1.57E-5 | 1448 ±1 | 159 ±6 | 63 | 50 | 5.56 |
| **6** | **BPAPF** (Lumtec) | 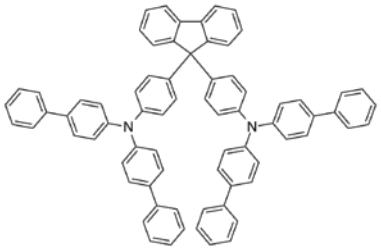 *N*,*N*′-diphenyl-*N*,*N*′-bis(9,9-dimethyl-fluoren-2-yl)-benzidine | 3.98E-5 | 1548 ±3 | 175 ±10 | 64 | 55 | 5.80 |
| **7** | **4P-TPD** (Sensient) | 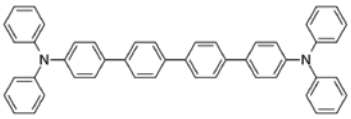 4,4‴-bis(*N*,*N*-dtphenylamino)-1,1′:4′,1″:4″,1‴-quaterphenyl | 1.97E-5 | 1576 ±4 | 187 ±13 | 82 | 72 | 5.88 |
| **8** | **MeO-TPD** (Sensient) | 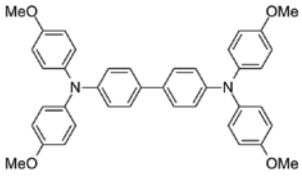 *N*,*N*,*N*′,*N*′-tetrakis(4-methoxyphenyl)-benzidine | 9.87E-6 | 1195 ±2 | 193 ±8 | 115 | 74 | 5.23 |
| **9** | **TCTA** (Sensient) | 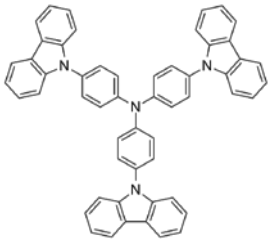 4,4',4''-tris(carbazol-9-yl)-triphenylamine | 2.16E-6 | 1507 ±5 | 199 ±13 | 129 | 114 | 6.06 |
| **10** | **BF-DPB** (Synthon) | 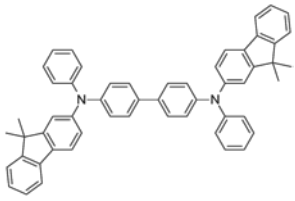 | 3.00E-6 | 1342 ±2 | 202 ±6 | 106 | 88 | 5.50 |

| | | | | | | | | |
|---|---|---|---|---|---|---|---|---|
| | | *N,N′*-diphenyl-*N,N′*-bis(9,9-dimethyl-fluoren-2-yl)-benzidine | | | | | | |
| **11** | **DMFL-NPD** (Lumtec) | 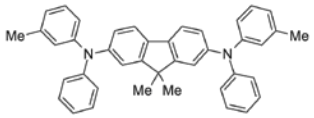 9,9-dimethyl-*N*,*N′*-diphenyl- *N*,*N′*-di-*m*-tolyl-9*H*-fluorene-2,7-diamine | 3.70E-7 | 1272 ±2 | 230 ±5 | 178 | 147 | 5.39 |
| **12** | **Spiro-MeO-TPD** (Lumtec) | 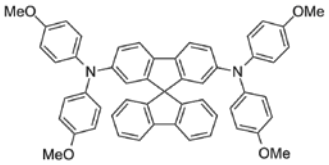 2,7-bis[*N,N*-bis(4-methoxy-phenyl)amino]9,9-spiro-bifluorene | 5.98E-7 | 1132 ±3 | 232 ±12 | 106 | 62 | 5.09 |
| **13** | **DH4T** (University Ulm) | 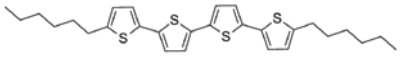 5,5‴-dihexyl-2,2′:5′,2″:5″,2‴-quarterthiophene | 1.26E-6 | 1516 ±2 | 234 ±13 | 173 | 75 | 5.72 |
| **14** | **DH6T** (University Ulm) | 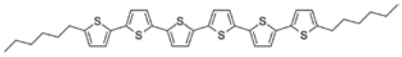 5,5‴″-dihexyl-2,2′:5′,2″:5″,2‴:5‴,2⁗:5⁗,2⁗′-sexithiophene | 1.69E-6 | 1444 ±2 | 281 ±19 | 156 | 76 | 5.58 |
| **15** | **α-6T** (Lumtec) | 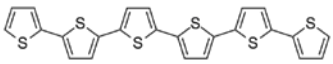 2,2′:5′,2″:5″,2‴:5‴,2⁗:5⁗,2⁗′-sexithiophene | 8.68E-6 | 1500 ±2 | 282 ±14 | 160 | 86 | 5.59 |
| **16** | **m-MTDATA** (Lumtec) | 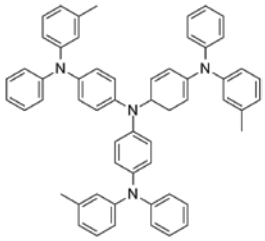 4,4′,4″-tris(3-*m*-tolyl-phenylamino)-triphenylamine | 1.08E-8 | 957 ±1 | 407 ±7 | 231 | 205 | 5.24 |

| | | | | | | | | |
|---|---|---|---|---|---|---|---|---|
| **17** | **2-TNATA** (Sensient) | 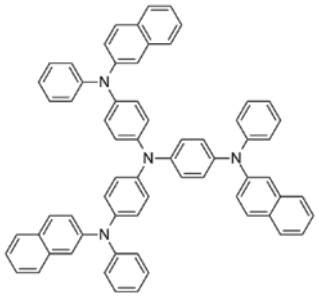 4,4',4''-tris(2-naphthylphenylamino)-triphenylamine | 1.93E-8 | 1011 ±1 | 417 ±13 | 195 | 171 | 5.29 |
| **18** | **BDTA-BT** (Georgia Institute of Technology) | 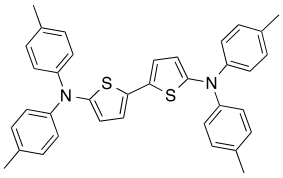 5,5'-bis(*N,N*-di-*p*-tolylamino)-2,2'-bithiophene | 6.44E-10 | 999 ±3 | 475 ±36 | 377 | 328 | 5.37 |

## 2. Hole only devices

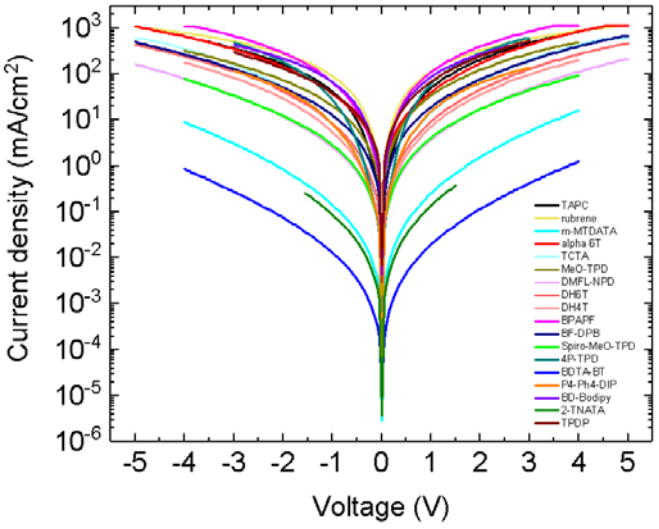


Figure S1. Absolute current density vs applied voltage of 18 hole-only devices. The curves are symmetric.

The J-V curves of the hole only devices were fitted using the Murgatroyd equation for space charge limited current:

$$J(V) = \frac{9}{8}\frac{\varepsilon\mu_0}{L^3}V^2 e^{0.89\gamma\sqrt{\frac{V}{L}}} \qquad (1)$$

## 3. Dependence of mobility on $E_{CT}$ and $\Lambda_D'^{calc}$

In the following, hole mobilities are shown in two graphs for materials with similar $\Lambda_D'^{calc}$ and varying $E_{CT}$ and vice versa. It is evident that the dominating parameter affecting mobility is $\Lambda_D'^{calc}$ as multiplying $\Lambda_D'^{calc}$ by a factor 3 changes the mobility by 5 orders of magnitude. Varying $E_{CT}$ by a factor 2 instead leaves the mobility almost unchanged.

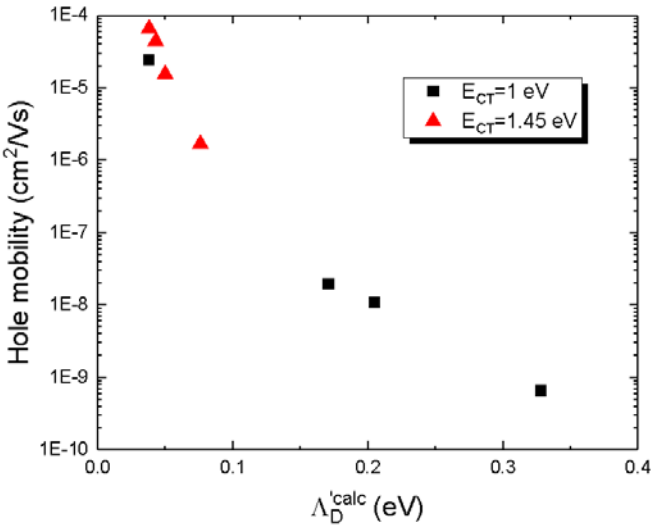


Figure S2 Mobilities for materials with similar $E_{CT}$=1 eV or $E_{CT}$=1.45 eV and varying $\Lambda_D'^{calc}$.

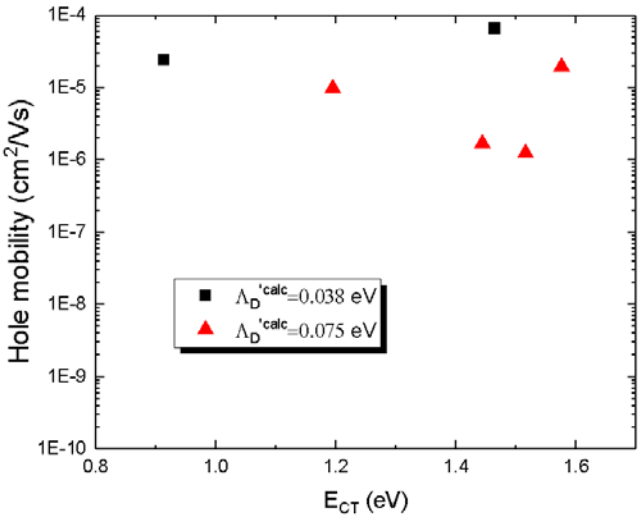


Figure S3 Mobilities for materials with similar $\Lambda_D'^{calc} = 0.038$ or $\Lambda_D'^{calc} = 0.075$ and varying $E_{CT}$.

# 4. Dark injection

A voltage step was applied on the samples and the current was monitored to get the peak current time. The mobility is then calculated from the current maximum time as:

$$\mu = 0.787 \frac{d^2}{t_{peak} V} \quad (2)$$

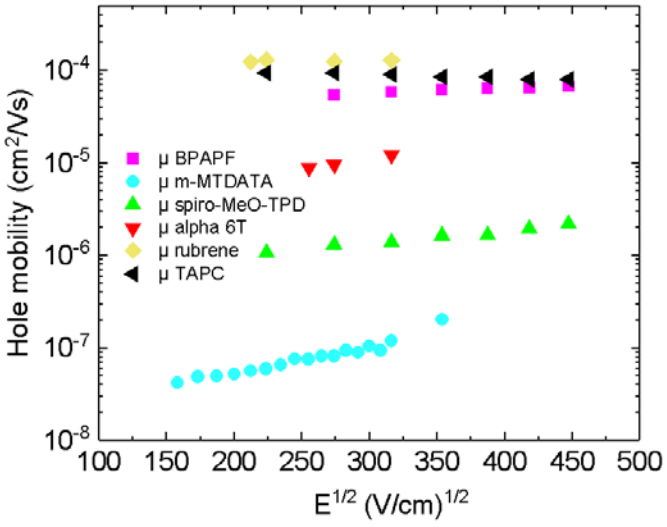


Figure S4 Hole mobilities obtained from dark injection transients.

The mobilities values were fitted with a Poole-Frenkel function to get the field-independent mobility $\mu_0$:

$$\mu(E) = \mu_0 e^{\gamma\sqrt{E}} \quad (3)$$

which is in agreement with the hole mobility obtained from SCLC measurements on hole-only devices:

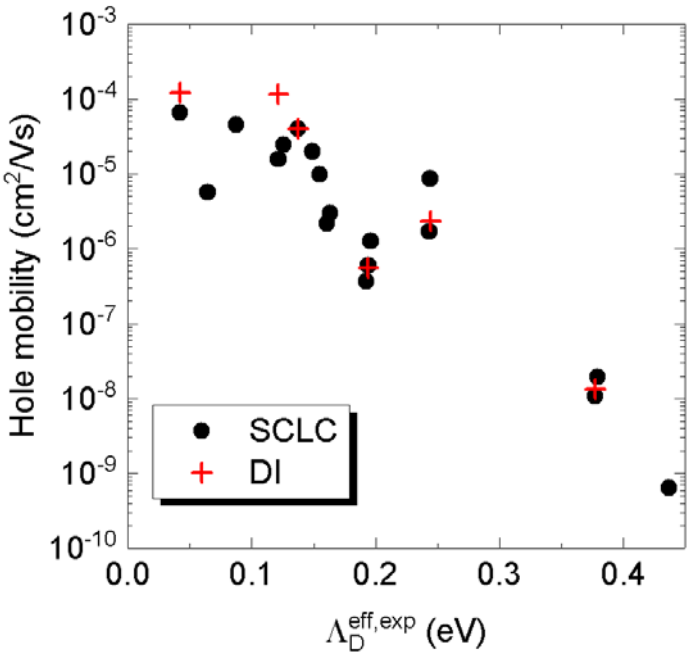


Figure S5 The mobility values determined by dark injection (DI), shown as red crosses, are in good agreement with the values obtained from SCLC measurements on hole-only devices, which are shown as black dots.

## 5. Superexchange transfer rate correlation with trap depth

Charge transport in amorphous organic semiconductor is commonly described as an incoherent process: thermally assisted tunneling (hopping) between localized states on individual molecules. Superexchange is a coherent process, tunneling happen between two lower laying energy units through a higher energy "bridge" unit, in which the carrier resides only virtually. The effective superexchange transfer integral, to be combined with the direct transfer integrals $H_{AC,0}$ according to $H_{AC} \cong H_{AC,0} + H_{AC,SE}$, directly depends on $E_{tr}$ as

$$H_{AC,SE} = \sum_{i=1}^{N} \frac{H_{AB_i,0} H_{B_iC,0}}{\Delta E_{AB_iC}} \qquad (4)$$

where the energy denominator in eq (4) is given by

$$\Delta \mathrm{E}_{ABC} = E_{B,0} - \frac{E_{A,0} + E_{C,0}}{2} + \Lambda_{C_{60}} \qquad (5)$$

and is related to the energy $E_{B,0}$ of the system in its virtual state with the charge on molecule B (and $\Lambda_{C_{60}}$ the relaxation energy of $C_{60}$).[1,2] In our case of equal donors, eq (5) simplifies because $E_{A,0} = E_{C,0} = -IP_D$, thus yielding direct proportionality to the donor IP ($\Delta \mathrm{E}_{ABC} \cong E_{tr}$), which means that the superexchange transfer integral may depend on the activation energy $H_{AC,SE} \propto 1/E_{tr}$ and the hole-transfer rate for superexchange $\propto 1/E_{tr}^2$ accordingly.

## 6. Schematic representation of the two proposed hole transport mechanism

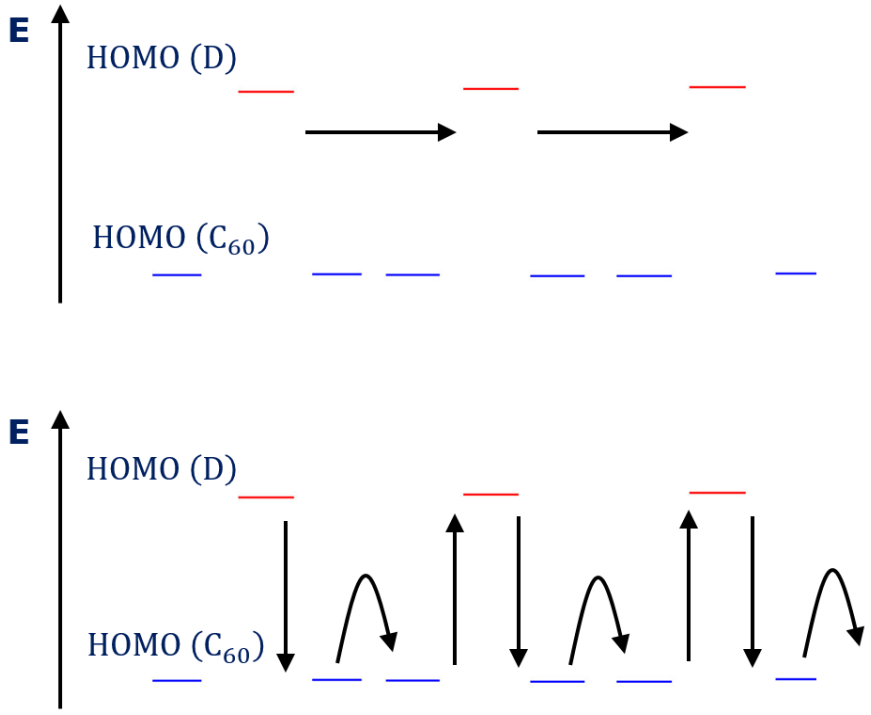


Figure S6 Schematic representation of the two proposed hole transport mechanis. Above holes tunnel from one donor to another donor through the $C_{60}$ host. Below holes move by means of thermally assisted jumps from the highest occupied molecular orbital (HOMO) of the donor to the HOMO of the neighboring $C_{60}$. Since $C_{60}$ is able to transport holes, those might then be transported in the fullerene phase, until they are trapped at another donor molecule.

# 7. Methods

**Device preparation:** Organic solar cells were prepared with a photo-active layer consisting of diluted donor:$C_{60}$ blends, employing 18 different donor molecules with varying frontier energy level offsets (for information regarding the donors see Table S1 in SI). The device architecture is as follows: the substrate is glass with a pre-structured ITO contact (Thin Film Devices, USA). 2 nm of $MoO_3$ are deposited to adjust the ITO work function and to form an Ohmic hole contact. The active layer is thermally evaporated at ultra-high vacuum (base pressure < $10^{-7}$ mbar) and consists of 50 nm small molecule electron donor diluted at ~6 mol% in $C_{60}$. The solar cell is then finalized with 8 nm of Bathophenanthroline (BPhen, abcr GmbH, Germany), used as electron contact, and 100 nm of Al. The device is defined by the geometrical overlap of the bottom and the top contact with an active area of 6.44 $mm^2$. To avoid exposure to ambient conditions, the organic part of the device is covered by a small glass substrate, glued on top.

**Hole only devices:** For hole space charge limited current mobility measurements, single carrier devices were prepared, where the top cathode (BPhen, Al) was substituted with another layer of $MoO_3$ 3 nm thick, followed by 100 nm of Ag.

For dark injection measurements the samples' active layers were thicker (200 nm).

**Sensitive EQE measurements:** The light of a quartz halogen lamp (50 W), chopped at 140 Hz, is coupled into a monochromator (Cornerstone 260 1/m, Newport). The resulting monochromatic light is focused onto the solar cell, its current at short-circuit conditions is fed to a current pre-amplifier before it is analyzed with a lock-in amplifier (7280 DSP, Signal Recovery, Oak Ridge,

USA). The time constant of the lock-in amplifier was chosen to be 1 s and the amplification of the pre-amplifier was increased to resolve low photocurrents. The EQE is determined dividing the photocurrent of the organic solar cell by the flux of incoming photons, which was obtained with a calibrated silicon (Si) and/or indium-gallium-arsenide (InGaAs) photodiode.

**Theoretical calculations:** All calculations were performed within density functional theory using the Gaussian09 software package.[3] Structure relaxations and calculations of (reduced) relaxation energies use the B3LYP hybrid functional and the 6-311G** basis set.[4-7] Relaxation energies of the donor molecules are obtained from the adiabatic potential energy surface of the neutral state according to $\Lambda_D = E(q_+) - E(q_0)$, with $E(q_+)$ the energy of the neutral molecule in the relaxed geometry of the cationic state and $E(q_0)$ the ground state energy.[8]

Each normal mode $j$ contributes to the relaxation process according to a dimensionless electron-phonon coupling constant $g_j$ with $\Lambda_D = \sum_j \lambda_j = \sum_j g_j^2 \hbar\omega_j$. The coupling constants $g_j$ are extracted from an expansion of the relaxed neutral structure by the normal mode vectors followed by an evaluation of the linear variation in HOMO energy according to reference (9) . Here, we apply a scaling factor of 0.967 for the frequencies of the vibrational modes $\hbar\omega_j$, but we keep the relaxation energies $\lambda_j$ by increasing the coupling constants $g_j$ by a factor of $\sqrt{1/0.967}$.[10] To extract the reduced relaxation energy $\Lambda'_D$, we subtract the contributions from high energy quantum modes ($\hbar\omega_j$ =1000 cm$^{-1}$) from $\Lambda_D$.[11]

Ionization potentials of the donor molecules in the solid state are estimated from vacuum values $IP_0$ using[12,13]

$$\mathrm{IP}' = IP_0 + P - \Lambda_\mathrm{D} \tag{6}$$

with the polarization energy $P$ obtained as

$$P = \frac{e^2}{8\pi\varepsilon_0 r_\mathrm{ion}}\left(\frac{1}{\varepsilon_\mathrm{rel}} - 1\right) < 0 \tag{7}$$

We assume $\varepsilon_\mathrm{rel} = 4.4$ being the dielectric constant of $C_{60}$ [14] because of the low donor content. $r_\mathrm{ion}$ and $IP_0$ are extracted from DFT calculations using the M06-2X hybrid functional and the cc-pVTZ basis set.[15-17]

# References


(1) Symalla, F.; Friederich, P.; Massé, A.; Meded, V.; Coehoorn, R.; Bobbert, P.; Wenzel, W. Charge Transport by Superexchange in Molecular Host-Guest Systems. *Phys. Rev. Lett.* ***2016***, 117, 276803.

(2) Massé, A.; Friederich, P.; Symalla, F.; Liu, F.; Meded, V.; Coehoorn, R.; Wenzel, W.; Bobbert, P. A. Effects of Energy Correlations and Superexchange on Charge Transport and Exciton Formation in Amorphous Molecular Semiconductors: an Ab Initio Study. *Phys. Rev. B* ***2017***, 95, 115204.

(3) Frisch, M. J.; Trucks, G. W.; Schlegel, H. B.; Scuseria, G. E.; Robb, M. A.; Cheeseman, J. R.; Scalmani, G.; Barone, V.; Mennucci, B.; Petersson, G. A.; et al. Gaussian 09, Revision D.01. *Gaussian, Inc.: Wallingford, CT* ***2009***.

(4) Becke, A. D. Density-Functional Exchange-Energy Approximation with Correct Asymptotic Behavior. *Phys. Rev. A* ***1988***, 38, 3098.

(5) Becke, A. D. Density-Functional Thermochemistry. III. The Role of Exact Exchange. *J. Chem. Phys.* ***1993***, 98, 5648–5652.

(6) Becke, A. D. A New Mixing of Hartree–Fock and Local Density-Functional Theories. *J. Chem. Phys.* ***1993***, 98, 1372–1377.

(7) Krishnan, R.; Binkley, J. S.; Seeger, R.; Pople, J. A. Self-Consistent Molecular Orbital Methods. XX. A Basis Set for Correlated Wave Functions. *J. Chem. Phys.* ***1980***, 72, 650–654.

(8) Coropceanu, V.; Cornil, J.; da Silva Filho, D. A.; Olivier, Y.; Silbey, R.; Brédas, J.-L. Charge Transport in Organic Semiconductors. *Chem. Rev.* ***2007***, 107, 926–952.

(9) Ortmann, F.; Radke, K. S.; Günther, A.; Kasemann, D.; Leo, K.; Cuniberti, G. Materials Meets Concepts in Molecule-Based Electronics. *Adv. Funct. Mater.* ***2014***, 25, 1933–1954.

(10) Scott, A. P.; Radom, L. Harmonic Vibrational Frequencies: An Evaluation of Hartree-Fock, Møller-Plesset, Quadratic Configuration Interaction, Density Functional Theory, and Semiempirical Scale Factors. *J. Phys. Chem.* ***1996***, 100, 16502.

(11) Vandewal, K.; Benduhn, J.; Schellhammer, K. S.; Vangerven, T.; Rückert, J. E.; Piersimoni, F.; Scholz, R.; Zeika, O.; Fan, Y.; Barlow, S.; et al. Absorption Tails of Donor:$C_{60}$ Blends Provide Insight Into Thermally Activated Charge-Transfer Processes and Polaron Relaxation. *J. Am. Chem. Soc.* ***2017***, 139, 1699–1704.

(12) Wang, X.; Zhang, F.; Schellhammer, K. S.; Machata, P.; Ortmann, F.; Cuniberti, G.; Fu, Y.; Hunger, J.; Tang, R.; Popov, A. A.; et al. Synthesis of NBN-Type Zigzag-Edged Polycyclic Aromatic Hydrocarbons: 1,9-Diaza-9a-Boraphenalene as a Structural Motif. *J. Am. Chem. Soc.* ***2016***, 138, 11606–11615.

(13) Scholz, R.; Luschtinetz, R.; Seifert, G.; Jägeler-Hoheisel, T.; Korner, C.; Leo, K.; Rapacioli, M. Quantifying Charge Transfer Energies at Donor–Acceptor Interfaces in Small-Molecule Solar Cells with Constrained DFTB and Spectroscopic Methods. *J. Phys.: Condens. Matter* ***2013***, 25, 473201.

(14) Hebard, A. F.; Haddon, R. C.; Fleming, R. M.; Kortan, A. R. Deposition and Characterization of Fullerene Films. *Appl. Phys. Lett.* ***1991***, 59, 2109–2111.

(15) Zhao, Y.; Truhlar, D. G. The M06 Suite of Density Functionals for Main Group

Thermochemistry, Thermochemical Kinetics, Noncovalent Interactions, Excited States, and Transition Elements: Two New Functionals and Systematic Testing of Four M06-Class Functionals and 12 Other Functionals. *Theor. Chem. Acc.* ***2008***, 120, 215–241.

(16) Dunning, T. H., Jr. Gaussian Basis Sets for Use in Correlated Molecular Calculations. I. The Atoms Boron Through Neon and Hydrogen. *J. Chem. Phys.* ***1989***, 90, 1007–1023.

(17) Kendall, R. A.; Dunning, T. H., Jr.; Harrison, R. J. Electron Affinities of the First-Row Atoms Revisited. Systematic Basis Sets and Wave Functions. *J. Chem. Phys.* ***1992***, 96, 6796–6806.